THE SEISMIC PERFORMANCE OF STEEL-ENCASED REINFORCED CONCRETE BRIDGE PILES

R.J.T. Park (I)
M.J.N. Priestley (I)
W.R. Walpole (I)
Presenting Author: W.R. Walpole

SUMMARY

An experimental and theoretical investigation into the seismic performance of steel-encased reinforced concrete bridge piles is described. Six large-scale test specimens were tested under cyclic lateral displacement-controlled loading. Variables included the axial load level, inclusion or exclusion of internal reinforcing cages, and the influence of casing discontinuity at the critical flexural sections. Sound seismic performance was observed in all of the models and good agreement between predicted and observed ultimate behaviour was obtained.

INTRODUCTION

It has not been common practice to design bridge pile systems for ductility under seismic attack. However, the vagaries of soil-pile interaction, fluctuations in river bed level, and the dynamic response of structural systems common in bridging, imply that plastic hinging of the piles may be impossible to prevent. Because of the common usage of steel-encased reinforced concrete piles for bridge foundations in New Zealand, their seismic performance is of particular importance.

Extensive testing of reinforced concrete members under simulated seismic attack (Ref. 1) had shown that sound performance was dependent on the provision of adequate spiral reinforcement. This suggested that steel encased concrete piles which have well-confined concrete cores would perform adequately. However, the theoretical structural response of cased piles is complicated by the state of biaxial stress in the casing; which is subjected to shear stresses, longitudinal stresses from axial and flexural loading in the pile, and hoop stresses from confinement of the encased concrete. The interaction of these stresses under post-elastic cyclic loading is extremely complicated. An additional complication is the potential for local buckling of the casing within the plastic hinge region.

In an attempt to quantify these effects, six model piles were tested and the experimental results were compared with theoretical predictions based on moment-curvature analyses under monotonic loading.

(I) Department of Civil Engineering,
University of Canterbury,
New Zealand.

DESCRIPTION OF TEST UNITS

The six circular test units all had the same basic dimensions of outside diameter D = 360 mm, total height 3.9 m, and casing wall thickness t = 5 mm. They were essentially tested as vertical axially-loaded beams with a central horizontal load (see Fig. 1). Axial load was applied by a 10 MN DARTEC electrohydraulic Universal Testing Machine, and lateral load by a 500 kN MTS actuator. The central stubs were heavily reinforced to ensure that critical sections occurred in the piles at the faces of the stubs.

The test units were arranged in three pairs with one of each pair tested at an axial load ratio, $P/(f'_c A_g)$, of 0.1 and the other at 0.3. Units 1 and 2, consisted of continuous concrete-filled tubes without internal reinforcement. Units 3 and 4 consisted of continuous concrete-filled tubes with internal longitudinal and spiral reinforcement. Units 5 and 6, simulating typical bridge abutment piles, contained internal reinforcement and were constructed with the casing embedded only 50 mm into the central stub, leaving a gap of 300 mm in the continuity of the casing at the midheight of the units. A typical prototype section, together with the model section, is shown in figure 2; and the spiral reinforcement spacing, casing steel and longitudinal reinforcement are detailed in figure 3.

The spiral reinforcement was designed to New Zealand requirements (Ref. 2) conservatively ignoring the presence of the casing. The thickness of the steel tube is required (Ref. 2) to satisfy:

$$t \geq D \sqrt{f_y/(8E_s)} \qquad (1)$$

where f_y = steel yield stress and E_s = Young's modulus for steel. Equation 1 gave a value of $t > 5.4$ mm compared with the actual value of 5 mm. A summary of the concrete strengths, f'_c, and steel yield stresses, f_y, is given on Table 1 together with other test unit details. Full details are available in Reference 3.

EXPERIMENTAL AND THEORETICAL RESULTS

Test Procedures

The horizontal load was cycled at a slow rate in a displacement controlled pattern. An initial cycle of static loading to ± 75% of the theoretical ultimate lateral load, H_{ACI}, was applied. From the resulting horizontal load-deflection plot an experimental value for the yield displacement, Δ_y was obtained by multiplying the peak displacement by 1.333. For this purpose H_{ACI} was based on strain compatability, using the measured steel yield stresses, f_y, the concrete unconfined compression failure stress f'_c, a maximum concrete strain of 0.003, the A.C.I. stress block for concrete in compression and no strength reduction factor (ϕ = 1.0). The casing steel was ignored in strength computations for units 5 and 6. Following the initial cycle a minimum of two complete cycles, each to displacement ductility levels μ $(=\Delta/\Delta_y)$ of ±2, ±4, ±6 were applied, and subsequently dynamic loading at a frequency of 0.125 Hz was undertaken.

General Behaviour

The performance of units 1 to 4 which had continuous casing, was strongly influenced by the development of local buckling in the casing at the critical sections. The bulges which extended over an axial length of 60 mm, formed on the first cycle to a ductility level of $\mu = 4$, and grew to a maximum outstand of approximately 15 mm by the end of static testing. In the case of units 1 and 2, which did not possess internal reinforcing, horizontal fracturing of the casing occurred in the dynamic testing phase, after 5 cycles at a ductility level of $\mu = \pm 4.7$. Subsequent removal of the casing, for units 1 to 4, showed a very short zone of crushed core concrete corresponding to the positions of casing bulging.

Units 5 and 6, with discontinuous casings, performed very well. Unit 6, which had R10 (10 mm diameter plain bar) spiral reinforcement at 35 mm centers, in the critical plastic regions, appeared practically indestructible. While unit 5, which had R10 spiral reinforcement at 70 mm centers, was performing well after its extensive static cycling, there was visual evidence of slipping of the casing relative to the internal core concrete. Thus it was clear that the casing and the internal core concrete were not acting compositely, and that the critical section was at the curtailment of the casing, 50 mm inside the central stub.

Load-Deflection Response

The lateral load-lateral deflection responses for static loading of units 1, 3 and 6 are illustrated in figures 4a, 4b and 4c respectively. These diagrams also show theoretical predictions. The theoretical capacity, H_{ACI}, is indicated, with a sloping line which takes into account the $P-\Delta$ effect from axial load.

Theoretical responses based on monotonic loading moment-curvature analyses are also shown. For units 1 to 4 there are three predictions. The first prediction is based on capacity of the steel tube alone. The second prediction, labelled 'theoretical lower bound', assumes that the concrete stress-strain response is enhanced by confinement due only to any spiral reinforcement, whilst the tube's stress-strain response is identical to its uniaxial response. The third prediction, labelled 'Theoretical upper bound' assumes that the concrete stress-strain response is enhanced by the confinement provided by the tube as well as any spiral reinforcement that may be present with the steel having its full uniaxial strength available for flexure. The model adopted for confined concrete was that due to Leslie and Park (Ref. 4), and the steel model used modelled the strain-hardening range as well as the normal elastic-plastic range.

For units 5 and 6 the theoretical prediction was based on the properties of the reinforced concrete section enhanced by the confining effect of the steel tube. Thus the casing which extended only 50 mm into the stub was assumed not to contribute to flexural strength of the pile.

The hysteresis loops for units 1 to 4 all showed that strength in excess of the theoretical ultimate strength, H_{ACI}, taking into account P-Δ effect, is available at high displacements. This was despite the significant stiffness degradation through the middle range of deflections which was due to the concrete cracks closing and the casing bulges restraightening under reversed loading.

The hysteresis loops for units 5 and 6 exhibited excellent behaviour with little strength and stiffness degradation under cyclic loading and strength well in excess of H_{ACI}. The loops were significantly pinched in the middle range of the deflections. This was probably caused by shear deformation, wide opening of cracks and lack of end bearing for the casing. Subsequent to the static testing shown in figure 4a, 81 dynamic cycles at $\mu = \pm 20$ were performed and then a static half cycle to $\mu = -40$ was performed with the unit still failing to degrade signficantly.

Table 2 summaries the maximum experimental and theoretical moments and yield deflections, together with maximum displacement ductility obtained above ($|\mu_T|$) and beneath ($|\mu_B|$) the central stub and the cumulative displacement ductility demand ($\Sigma|\mu|$). In particular it should be noted that units 1 to 4 were approximately 22% stronger than predicted by conventional theory with peak responses lying between theoretical upper and lower bound curves indicating effective composite action. Units 5 and 6 exhibited large overstrength well in excess of the theoretical prediction, as a result of casing end-bearing and the confining effect of the central stub.

Ductility Criteria

In New Zealand, current seismic design philosophy (Ref. 5 and 6) implies that ductile bridge structures should not suffer significant strength degradation at displacement ductility factors of 6 or cumulative displacement ductility factors $\Sigma|\mu|$ of 32 (i.e. 4 cycles at $\mu = \pm 4$). As can be seen from figure 4 and table 2, units 1 to 4 were satisfactory, whilst units 5 and 6 exceeded these criteria by a factor of at least 9. However the pinched nature of the hysteresis loops might imply that the prototype piles would be subjected to higher ductility levels, than those predicted on the assumption of elasto-plastic response.

Table 3 indicates the estimated maximum concrete compression strain (ε_c) and curvature ductility demand sustained by units 1 to 4 during static testing. Extremely high local compression strains and curvature ductilities in the vicinity of casing buckling will be noted.

CONCLUSIONS

The model steel-encased concrete piles exhibited satisfactory seismic performance, with ductility capacity exceeding current requirements for bridges in New Zealand. However, it was evident that local buckling of the casing, for the units with continuous casing, limited the potential for ductile performance. It is possible that prototype piles, with ratios of casing diameter to thickness greater than the value of 72 used in the test series, would perform less favourably. The New Zealand requirement, with regard to a minimum thickness of steel encasement as expressed in equation (1), is conservative for concrete-filled steel tubes.

The strength of specimens with continuous casing was approximately 22% greater than the theoretical strength based on 0.003 concrete strain, strain compatability and measured material properties. The strength of specimens, with discontinuous casing at the critical flexural sections was approximately 73% higher than a prediction based on the reinforced core alone.

ACKNOWLEDGEMENT

Financial assistance from New Zealand Railways and the University of Canterbury is gratefully acknowledged. This research was part of a Master of Engineering project by Park, supervised by Priestley and Walpole.

REFERENCES

1. Ang, R.G., Priestley, M.J.N. and Park, R., "Ductility of Reinforced Concrete Bridge Piers under Seismic Loading", Res. Rept. 81-3, Civil Eng. Dept., University of Canterbury, Christchurch, New Zealand, 1981, 109 pp.

2. "Code of Practice for the Design of Concrete Structures", NZS3101, Standards Association of New Zealand, Wellington, 1982, 127 pp.

3. Park, R.J.T., Priestley, M.J.N., Walpole, W.R., "The Seismic Performance of Steel Encased Reinforced Concrete Bridge Piles", Res. Rept. 82-12, Civil Eng. Dept., University of Canterbury, Christchurch, New Zealand, 1982, 158 pp + App.

4. Leslie, P.D., "Ductility of Reinforced Concrete Bridge Piers", Master of Engineering Report, University of Canterbury, Christchurch, New Zealand, 1974.

5. Berrill, J.B., Priestley, M.J.N., and Chapman, H.E., "Design Earthquake Loading and Ductility Demand", Bulletin of the New Zealand National Society for Earthquake Engineering, Vol. 13, No. 3, September 1980, pp. 232-242.

6. "Code of Practice for General Structural Design and Design Loadings for Buildings", NZS4203: 1976, Standards Association of New Zealand, 104 pp.

Specimen	f'_c	$\frac{P_e}{f'_c A_g}$	Longitudinal bars		5 mm Casing		Spiral Steel in Plastic Hinge Region	
			No. of D16 bars	f_y	Continuous	f_y	R10 Spacing	f_y
1	28	0.1	-	-	Yes	370	-	-
2	28	0.3	-	-	Yes	370	-	-
3	28	0.1	9	315	Yes	370	70	295
4	28	0.3	9	315	Yes	370	35	295
5	29	0.1	9	315	No 50 mm cap embedment	370	70	295
6	29	0.3	9	315	No 50 mm cap embedment	370	35	295
Units	MPa	-	-	MPa	-	MPa	mm	MPa

Table 1 : Test Unit Details.

Specimen	(1) $\frac{P}{f'_c A_g}$	Δy (mm)		MOMENT (kNm)						(10) Over-strength available from A.C.I.	$\Sigma\|\mu\|$		Max (13) $\|\mu_T\|$ or $\|\mu_B\|$
		(2) Experiment	(3) Theory	(4) Equivalent A.C.I.	(5) Moment Curvature at $\varepsilon_c = 0.003$	(6) Maximum experimental	(7) Upper bound	(8) Lower bound	(9) Confined		(11) Static	(12) Dynamic	
1	0.1	14.4	14.4	285	283	335	341	313	-	18	51	56	8.3
2	0.3	12.6	13.9	299	304	376	383	-	-	26	67	43	7.8
3	0.1	14.5	14.3	334	341	397	406	392	-	19	53	131	7.9
4	0.3	14.3	14.3	344	355	435	460	432	-	26	81	-	12.4
5	0.1	3.2	9.7(3.3)	100	103	187	-	-	135	87	303	-	67.1
6	0.3	3.2	8.5(3.9)	128	132	216	-	-	168	69	326	1620	104.4

Table 2 : Summary of Test Results.

Unit	Curvature Ductility Demand		ε_c (%)		Maximum of $\|\mu_T\|$ or $\|\mu_B\|$
	300 mm gauge length	concentrated at 60 mm long bulge	300 mm gauge length	concentrated at 60 mm long bulge	
1	20.2	101	4.2	21	8.3
2	15.6	78	4.7	24	7.8
3	20.5	103	4.7	24	7.9
4	22.2	111	3.6	18	12.4

Table 3 : Maximum Deformations.

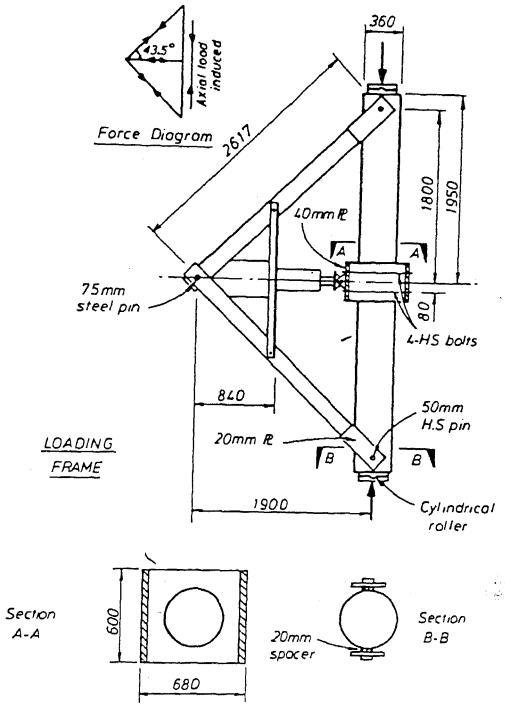

Fig. 1 : Test Unit in the Reaction Frame.

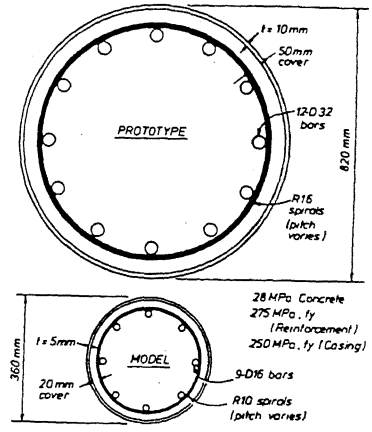

Fig. 2 : Model and Prototype Section.

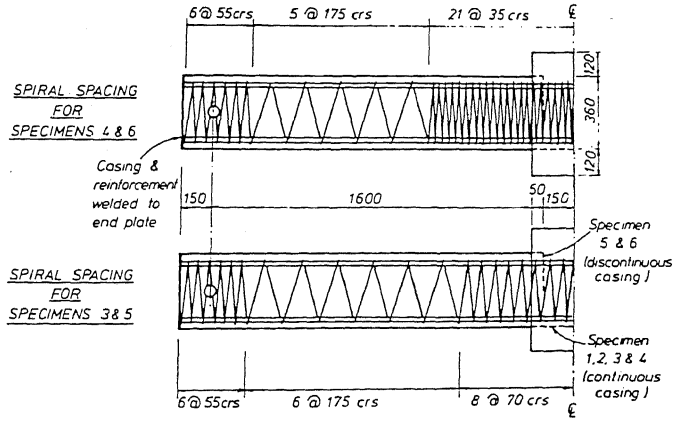

Fig. 3 : Spiral Reinforcement Spacing, and Casing Steel Embedment.

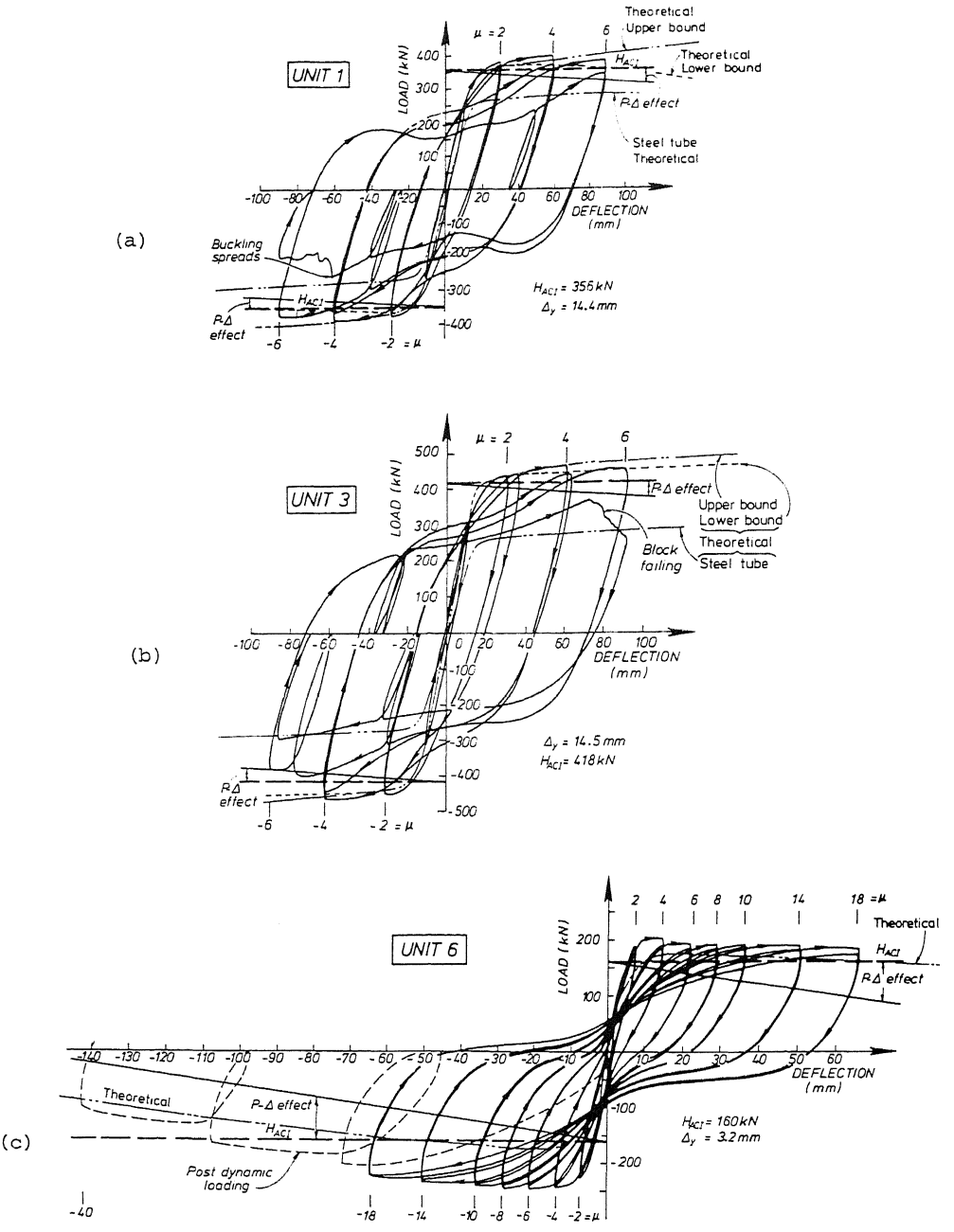

Fig. 4 : Static Cycling Lateral Load-Lateral Deflection Response.